AMERICAN SCIENTIFIC PUBLISHERS

Science of Advanced Materials
Vol. 6, pp. 1708–1715, 2014
(www.aspbs.com/sam)

ARTICLE

Facile Synthesis and Magnetic Properties of Hybrid-Phase Iron Oxide Nanoparticles by Polymer-Supported Nanoemulsion

Hong Qin Shao[1], Peng Hou[1], Xian Hong Wang[1], Xiao Liu[1], Xue Mei Li[1], Hong Ling Liu[1,*], and Jun Hua Wu[2,*]

[1]*Key Lab of Polyoxometalate Chemistry of Henan Province, Institute of Molecular and Crystal Engineering, School of Chemistry and Chemical Engineering, Henan University, Kaifeng 475001, China*
[2]*Pioneer Research Center for Biomedical Nanocrystals, Korea University, Seoul 136-713, South Korea*

ABSTRACT

We report a facile nanoemulsion synthesis of hybrid-phase iron oxide nanoparticles supported by poly(ethylene glycol)-block-poly(propylene glycol)-block-poly(ethylene glycol) (PEO-PPO-PEO). The FTIR spectra proves the PEO-PPO-PEO molecules sitting on the resulting nanoparticle surface, whereas the outcome from the morphological analysis gives the nanoparticle shape, size and size distribution, showing an average particle size of ~7.4 nm with a tight monosize distribution. Moreover, the structural characterization exposes that the nanoparticles as prepared consist of three phases, orthorhombic FeO, cubic α-Fe and inverse spinel Fe_3O_4, with the crystallographic parameters of the new FeO phase identified as $a = 8.034$ Å, $b = 10.359$ Å, and $c = 12.341$ Å. In addition, the hybrid-phase iron oxide nanoparticles manifest well-defined soft ferromagnetic behaviour and the pertinent magnetic hysteresis curves are effectively assessed by modified tri-phase Langevin equations revealing three magnetic phases which correspond to the structural phases. The analysis, therefore, shows that such hybrid-phase iron oxide nanostructure entity covered by the biocompatible triblock copolymer is interesting for study in the polymorphism of iron oxides and prospective for potential application.

KEYWORDS: Nanoparticle, Nanoemulsion, Magnetic Property, Langevin Equation, Iron Oxide.

1. INTRODUCTION

Iron oxides have many fascinating phases, represented by wüstite (FeO), magnetite (Fe_3O_4), maghemite (γ-Fe_2O_3), and hematite (α-Fe_2O_3), and are omnipresent in nature occurring in various important geological and biological processes.[1–3] In nanostructured forms, a wide range of iron oxides have been tapped for basic mechanism and potential applications such as in magnetic resonance imaging, hyperthermia treatment for malignant cells, chemotherapy, manipulating cell membranes, magnetic separation and cell sorting, drug and gene delivery because of their unique magnetic properties and biocompatibility, as well as catalysis, environmental issues and implication in geological processes.[4–10] In particular, FeO or wüstite is an antiferromagnetic material in bulk with a Néel temperature T_N ~200 K and can be metastable to undergo a disproportionate reaction to metallic iron (α-Fe) and magnetite (Fe_3O_4), in addition to many other fascinating physical, chemical, thermal, and mechanical properties.[1] The metastability of the material under ambient conditions thus offers feasible routes producing mixed-phase or hybrid-phase nanoparticles by controlling the reaction parameters to tune, for examples, the corresponding magnetic properties through the composition variation and/or particle size. Extensive research has been fruitfully conducted to make colloidal FeO nanoparticles, usually in a nonstoichiometric composition which can result in phase transformation, complex defect structures, defect-related physicochemical properties and other interesting phenomena on the nanoscale.[1, 11–18]

Surface modification is an imperative issue which may not only tailor the surface properties appealing to fundamental study but also receive practical use, for instance, a biocompatible, functionalized surface is rigorously probed for biomedical purposes. Since the preparation and storage of nanoparticles are in a colloidal form, the stability of the colloid is of utmost importance. In addition to the usual flocculation due to van der Waals forces, moreover, iron oxide nanoparticles are magnetically attracted themselves, resulting in increased aggregation. Often nanoparticles

*Authors to whom correspondence should be addressed.
Emails: hlliu@henu.edu.cn, feitianshenhu@yahoo.com
Received: 28 January 2014
Accepted: 14 March 2014

are synthesized by means of small organic molecules like oleic acid, which is hydrophobic and later substituted by a hydrophilic reagent that is suitable for biomedical purpose that proceeds in an aqueous medium and requires the biocompatibility of the reagent. The substitution is normally completed through a secondary surface modification which commonly has obvious disadvantages as a consequence of involving a multiple-step, time-consuming process. Thus, natural coating of nanoparticle surfaces by biofriendly molecules is vastly crucial for future biomedical applications, especially *in-situ* during the fabrication of the nanoparticles. Furthermore, proper surface coating can protect the nanoparticles from oxidation and stabilize them in stock. In relevance, we have succeeded in the syntheses of various nanoparticles through nanoemulsion methodologies using diverse surfactants from small organic molecules to polymers, including poly(ethylene glycol)-block-poly(propylene glycol)-block-poly(ethylene glycol) (PEO-PPO-PEO) and poly(vinylpyrrolidone) (PVP).[7, 10, 19, 20] The PEO-PPO-PEO triblock copolymer and families encompass numerous distinct advantages such as aqueous solubility, non-charging, biocompatibility, and frequently used in the fields of drug solubilization and slow-release, wastewater treatment, preparation of mesoporous materials, animal cell culture, biomacromolecular separation, and nanoemulsion processes.[7, 10, 20–25] In a representative nanoemulsion process, the PEO-PPO-PEO molecules participate in the reaction as a surfactant, stabilize the colloidal solution of the nanoparticles formed, and yet can perform the role of a reductant. In this work, we report the one-pot nanoemulsion synthesis and magnetic properties of the PEO-PPO-PEO-coated hybrid-phase iron oxide nanoparticles with the PEO-PPO-PEO molecules as the surfactant. The FTIR survey elucidates the PEO-PPO-PEO coating on the surface of the resultant nanoparticles, whereas the structural analysis reveals that the nanoparticles are made up of three phases, orthorhombic FeO, cubic α-Fe and inverse spinel Fe_3O_4, as well as the morphological examination on the nanoparticle shape and size with a tight monosize distribution. In addition, the magnetic measurements illustrate that the PEO-PPO-PEO-coated hybrid-phase iron oxide nanoparticles have well-behaved magnetic response and the relevant hysteresis curves are evaluated by modified tri-phase Langevin equations, showing three magnetic phases which match to the structural phases.

2. EXPERIMENTAL DETAILS

2.1. Materials

The major precursor used for the nanoemulsion synthesis of the hybrid-phase iron oxide nanoparticles is iron (II) acetylacetonate ($Fe(acac)_2$, 99.9%). A triblock copolymer, poly(ethylene glycol)-block-poly(propylene glycol)-block-poly(ethylene glycol) (PEO-PPO-PEO, Mn = 5800) was used as the surfactant, with 1,2-hexadecanediol ($C_{14}H_{29}CH(OH)CH_2(OH)$, 90%) as the reducing agent. For comparison, iron (III) acetylacetonate ($Fe(acac)_3$, 99.9%) was employed to prepare magnetite (Fe_3O_4) nanoparticles. Other chemicals involve octyl ether ($C_8H_{17}OC_8H_{17}$, 99%) and solvents such as hexane and ethanol. All materials were purchased from Aldrich and were used as received without further processing.

2.2. Synthesis of PEO-PPO-PEO-Coated Hybrid-Phase Iron Oxide Nanoparticles

The synthesis of PEO-PPO-PEO-coated hybrid-phase iron oxide nanoparticles was conducted by the thermal decomposition of the precursor at an elevated temperature.[7, 10, 20] In a typical experiment, 0.1270 g of $Fe(acac)_2$ and 0.7856 g of PEO-PPO-PEO as the surfactant were dissolved in 10 ml octyl ether in a 250 ml flask containing 0.3234 g of 1,2-hexadecanediol as the reductant. Under vigorous stirring, the reaction mixture was first slowly heated to 125 °C from room temperature within 1 h and held for 2 h at 125 °C and then rapidly heated to 300 °C with 10 min and refluxed for 1 h at the temperature. After cooling down to room temperature, ethanol was added to the reacted mixture to precipitate the PEO-PPO-PEO-covered hybrid-phase iron oxide nanoparticles. The precipitated product was washed with ethanol/hexane (2:1) several times, and re-dispersed in hexane for further use.

2.3. Structural and Morphological Characterization

The morphology, particle size and size distribution of the PEO-PPO-PEO-coated hybrid-phase iron oxide nanoparticles was analyzed by transmission electron microscopy (TEM, JEM-100II), while the crystal structure of the nanoparticles was studied by powder X-ray diffraction (XRD, X'Pert Pro). In the Fourier transform infrared spectroscopy (FTIR) analysis, the washed PEO-PPO-PEO-coated hybrid-phase iron oxide nanoparticles, the PEO-PPO-PEO polymer and magnetite nanoparticles were crushed with a pestle in an agate mortar, separately. The FTIR spectra were recorded in the wavelength range of 4000–400 cm^{-1} using an Avatar 360 FTIR spectrometer (Nicolet Company, USA).

2.4. Measurements of Magnetic Properties and Analysis of Hysteresis Curves

Vibrating sample magnetometry (VSM, Lakeshore 7300) and Physical Property Measurement System (PPMS, Quantum Design) were applied to perform magnetic measurements on the dried samples to evaluate the magnetic properties of the nanoparticles as a function of applied magnetic field and temperature. In view of set-in coercivity, modified Langevin equations were employed to examine the hysteresis curves of the PEO-PPO-PEO-coated hybrid-phase iron oxide nanoparticles.

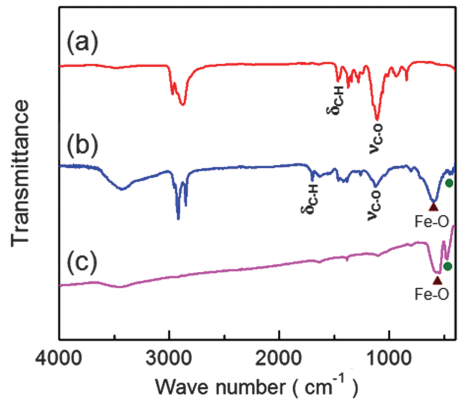

Fig. 1. FTIR spectra of (a) pure PEO-PPO-PEO molecules, (b) PEO-PPO-PEO-coated hybrid-phase iron oxide nanoparticles, and (c) magnetite nanoparticles. The triangles and discs indicate the vibration positions of Fe–O, together with the ν_{C-O} and ν_{C-H} bands from the polymer.

3. RESULTS AND DISCUSSION

The hybrid-phase iron oxide nanoparticles were prepared by the controlled nanoemulsion synthesis.[10,20] First, the iron precursor and 1,2-hexadecanediol were mixed under magnetic stirring and steady heating from room temperature to 125 °C with the polymer surfactant molecules in the solvent of octyl ether to form nano-micelles. Subsequently, the temperature was rapidly raised to 300 °C to generate the hybrid-phase iron oxide nanoparticles through the thermal decomposition of $Fe(acac)_2$. After the reaction, the resultant hybrid-phase iron oxide nanoparticles were separated from the supernatant and purified for further analysis.

The corroboration of presence of the PEO-PPO-PEO macromolecules on the surface of the hybrid-phase iron oxide nanoparticles in this work was obtained by FTIR on the purified nanoparticles in comparison to the pure polymer and magnetite nanoparticles.[1,21] Figure 1 compares the FTIR spectrum of the hybrid-phase iron oxide nanoparticles after purification with that of the PEO-PPO-PEO molecules used in the synthesis as the surfactant and the Fe_3O_4 nanoparticles. In Figure 1(a), the pure PEO-PPO-PEO molecules show a strong band at the position of $\sim$1108.9 cm^{-1} for the C—O—C stretching vibration of the ether bonding which commonly occurs in the range of 1250 cm^{-1} to 1000 cm^{-1} and a sharp band for the C—H bending vibration at the position of $\sim$1465.7 cm^{-1}.[21] As displayed in Figure 1(b), these characteristic vibration and bending modes recur in the FTIR spectrum of the hybrid-phase iron oxide nanoparticles, but instead shifting to the positions of $\sim$1126.3 cm^{-1} for the C—O—C stretching vibration and $\sim$1699.1 cm^{-1} for the C—H bending vibration, respectively. Moreover, the band shapes and absorption intensities differ noticeably from the pure PEO-PPO-PEO molecules to the hybrid-phase iron oxide nanoparticles. In mechanism, the blue-shifting and change in the band shape of the C—O—C stretching and C—H bending bands may engage the coordination of the

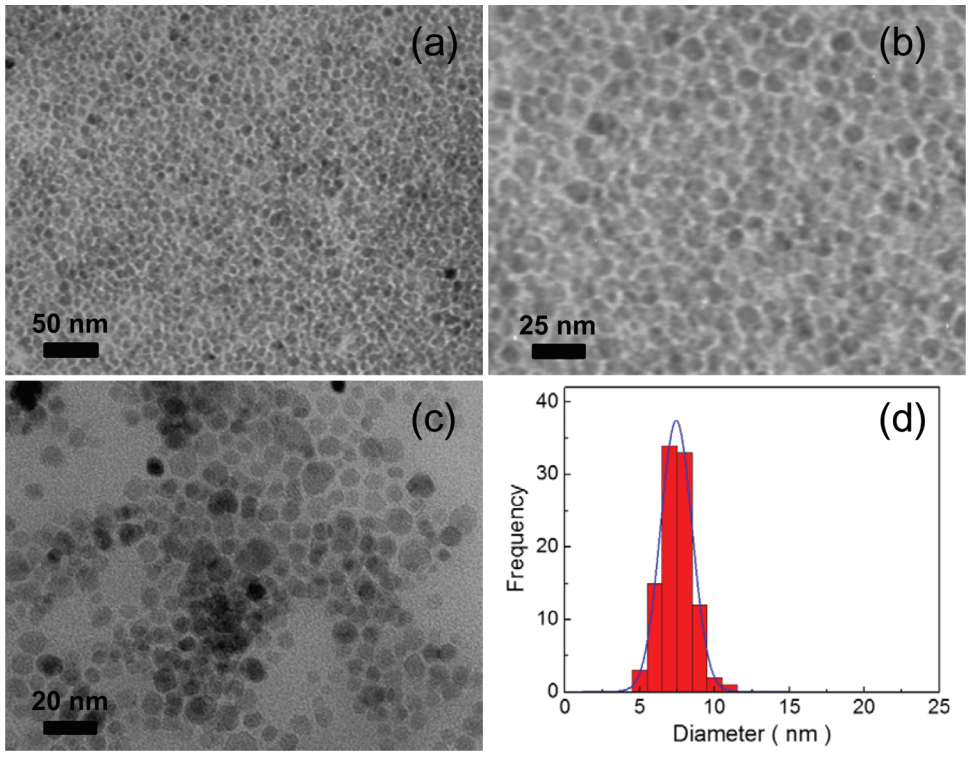

Fig. 2. TEM bright-field micrographs of (a), (b) the PEO-PPO-PEO-coated hybrid-phase iron oxide nanoparticles and (c) Fe_3O_4 prepared similarly, and (d) particle size distribution (in histogram) with Gaussian function fit (in curve).

oxygen atoms in the main chains to the Fe metallic atoms[26] and the physicochemical interactions between the polymer molecules and the oxide surface. As the excessive PEO-PPO-PEO molecules were removed by the purification process, the observation explicitly indicates the covering of the PEO-PPO-PEO molecules onto the surface of the hybrid-phase iron oxide nanoparticles, which can be further substantiated by the other relevant absorption bands in the spectra. Still, the characteristic band of Fe—O in the spectrum of the PEO-PPO-PEO-coated hybrid-phase iron oxide nanoparticles is located at ~592.1 cm^{-1} (Fig. 1(b)), which is analogous to the Fe—O bands of the magnetite nanoparticles positioning at ~580.5 cm^{-1} and ~474.3 cm^{-1} as shown in Figure 1(c) [refer to Chap. 7 of Ref. [1]], definitely distinct from the absence of absorption in the corresponding position in the spectrum of the pure PEO-PPO-PEO molecules (Fig. 1(a)).

The microstructure and grain size of the hybrid-phase iron oxide nanoparticles were acquired by XRD and TEM. Figures 2(a), (b) show the morphology and particle sizes of the PEO-PPO-PEO-coated hybrid-phase iron oxide nanoparticles acquired by TEM. Apparently, the nanoparticles are virtually uniform and spherical in shape, comparable to the magnetite nanoparticles prepared similarly (Fig. 2(c)). It is found that the hybrid-phase iron oxide nanoparticles have an average diameter of ~7.4 nm, with a narrow particle size distribution, and the histogram of the particle size can be satisfactorily fitted to a Gaussian function as indicated by the curve (Fig. 2(d)).

As shown in Figure 3(a), the crystal structure of the PEO-PPO-PEO-coated hybrid-phase iron oxide nanoparticles is obtained from the diffraction pattern recorded by XRD, against the pattern of Figure 3(b) for the magnetite nanoparticles as prepared in the same way from the precursor of $Fe(acac)_3$. In contrast to the inverse spinel cubic structure assigned to the magnetite nanoparticles as indexed in Figure 3(b), the diffraction pattern for the hybrid-phase iron oxide nanoparticles in Figure 3(a) can be divided into three phases, an orthorhombic phase for FeO, an inverse spinel cubic phase for Fe_3O_4, and a cubic phase for iron (α-Fe), which is distinctive from alternative approaches.[27]

(1) Analogous to the Fe_3O_4 nanoparticles made from $Fe(acac)_3$, the peaks as indicated by the symbols of squares at 30.21°, 35.54°, 37.13°, 43.19°, 47.36°, 53.60°, 57.11° and 62.72° are appropriately indexed to the Fe_3O_4 positions of (220), (311), (222), (400), (331), (442), (511) and (440) planes, which are in effect located in the positions of the corresponding material in bulk with no noticeable deviation within the error of measurements (JCPDS no. 87-0721).[20]

(2) At the position of 44.54° as labelled by the sign of diamond, the diffraction is indexed to the (110) plane of body-centered cubic iron, which corresponds to the lattice parameter a = 2.874 Å, slightly larger than $a = 2.866$ Å in bulk, which is probably as a result of nanosizing effects. These two phases arise from the disproportionate reaction of the metastable FeO according to $4\ FeO = Fe + Fe_3O_4$.[1]

(3) As designated by the inverted triangles with indexing in Figure 3(a), the rest of the diffractions in the PEO-PPO-PEO-coated hybrid-phase iron oxide nanoparticles are assigned to the orthorhombic phase of FeO with the lattice parameters of $a = 8.034$ Å, $b = 10.359$ Å and $c = 12.341$ Å.

The finding of the new orthorhombic phase of FeO in this work shows that a new synthetic approach is a powerful tool to introduce polymorphism and thus new properties in such a material.[1,28] Based on the full width at half maximum (FWHM) of the (311) Fe_3O_4 peak in Figure 3(a) by the Scherrer equation, furthermore, the average particle size of the nanoparticles is estimated to be ~7.8 nm, supposing that the broadening of the peaks in the XRD pattern is predominantly attributed to the finite-size of the nanoparticles.[29] The assessment is reasonably in consistence with the TEM observation discussed above.

As presented in Figure 4, the magnetic properties of the PEO-PPO-PEO-coated hybrid-phase iron oxide nanoparticles were measured by VSM and PPMS as a function of applied magnetic fields and temperature. According to Figure 4(a), the nanoparticles overall show soft ferromagnetic properties with a coercivity of ~15 Oe and magnetization of ~46.9 emu/g under ~30,000 Oe at room temperature, whereas the coercivity increases to ~208 Oe and the magnetization reduces to ~44.8 emu/g under ~30,000 Oe at 5 K. The inset shows the field response of the hybrid nanoparticles around the origin. The enhanced coercivity with the decreasing temperature is apparently the outcome of the thermal effects. However, the decrease in magnetization with the decreasing temperature clearly reflects the anti-ferromagnetic behavior of FeO in the PEO-PPO-PEO-coated hybrid-phase

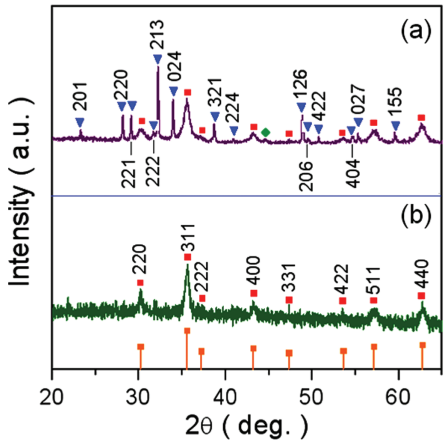

Fig. 3. XRD diffraction patterns of (a) the PEO-PPO-PEO-coated hybrid-phase iron oxide nanoparticles, consisting of orthorhombic FeO (in inverted triangles), cubic α-Fe (in diamond) and inverse spinel Fe_3O_4 (in squares), and (b) Fe_3O_4 prepared similarly, with JCPDS of bulk magnetite (in squares).

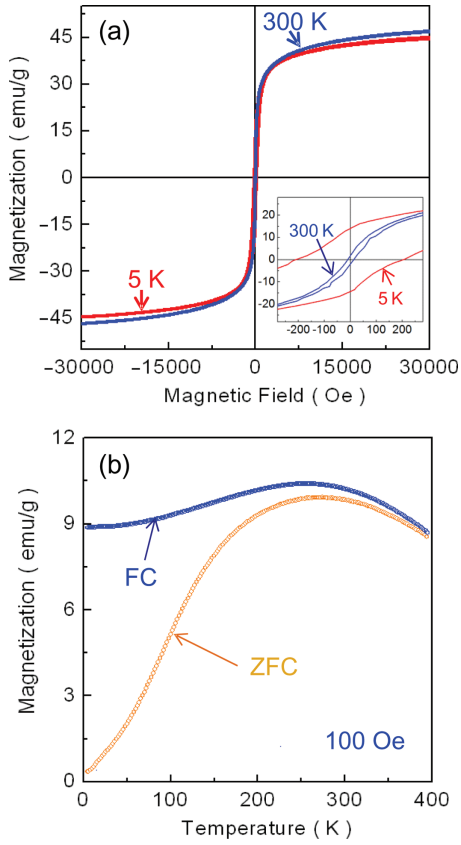

Fig. 4. Magnetic measurements of the PEO-PPO-PEO-coated hybrid-phase iron oxide nanoparticles. (a) Hysteresis curves recorded at 5 K and 300 K (Inset: Field response around the origin), and (b) FC and ZFC curves under the magnetic field of 100 Oe.

iron oxide nanoparticles, showing the pairing of the spins at the temperature of 5 K which is far below the Néel temperature.[1,14] Additionally, the superparamagnetic response of the nanoparticles is investigated by recording the magnetization–temperature (M–T) curves in two modes of field-cooling (FC) and zero-field-cooling (ZFC) under a given applied magnetic field of 100 Oe. As exhibited in Figure 4(b), the PEO-PPO-PEO-coated hybrid-phase iron oxide nanoparticles show an initial increase from of ~8.7 emu/g at ~395 K to the maximum of ~10.4 emu/g at ~257 K and then gradual decrease to ~8.9 emu/g at ~5 K with decreasing temperature in the FC mode, in contrast to the ZFC mode which reveals likewise an initial increase from of ~8.5 emu/g at ~395 K to the maximum of ~9.9 emu/g at ~274 K and afterward gradual freezing to ~0.3 emu/g at ~5 K with decreasing temperature. The phenomena as observed above clearly illustrate that the polymer-coated hybrid-phase iron oxide nanoparticles have the typical superparamagnetism of magnetic nanoparticles. For such nanoparticles under the applied magnetic field of 100 Oe, the blocking temperature is above 395 K and the freezing temperature reads ~274 K, with the signature temperature of electron pairing starting at ~257 K in reference to the FC curve.

As evidenced in the XRD analysis, the PEO-PPO-PEO-coated hybrid-phase iron oxide nanoparticles are composed of the three structural phases, which are anticipated in the resolution of the corresponding hysteresis curves as follows. The description of superparamagnetic magnetization processes has been afforded by the modified Langevin function in the consideration of setting-in coercivity in the case of the hybrid-phase iron oxide nanoparticles,[20,30]

$$\frac{M}{M_s} = \coth(\alpha') - \frac{1}{\alpha'} \quad (1)$$

$$\text{where } \alpha' = \frac{\mu(H - H_c)}{k_B T} \quad (2)$$

In the equations, M/M_S is the magnetization relative to the saturation magnetization, H the applied magnetic field, H_c the coercivity, T the temperature and k_B the Boltzmann constant.[20,30] As presented in Figures 5(a), (b) on the basis of Eq. (1), the single-phase fitting to the hysteresis curves at 300 K shows that the deviation is obvious over the whole range of the magnetic fields, suggesting that the nanoparticle ensemble is made up of more than one magnetic phase. Conversely, more reasonable description of the hysteresis curves at 300 K in Figure 4 is attainable by a bi-phase superposition of Eq. (3), signifying that the nanoparticle system is composed of two magnetic phases,[30]

$$M = M_S^1\left[\coth(\alpha_1) - \frac{1}{\alpha_1}\right] + M_S^2\left[\coth(\alpha_2) - \frac{1}{\alpha_2}\right] \quad (3)$$

or three magnetic phases,

$$M = M_S^1\left[\coth(\alpha_1) - \frac{1}{\alpha_1}\right] + M_S^2\left[\coth(\alpha_2) - \frac{1}{\alpha_2}\right] + M_S^3\left[\coth(\alpha_3) - \frac{1}{\alpha_3}\right] \quad (4)$$

In the equations, M_S^1, M_S^2, M_S^3, α_1, α_2 and α_3 are the fitting quantities corresponding to the magnetic phases 1, 2 or 3, respectively. The fittings extend over the whole range of the measurement quite well for both the bi-phase case (Fig. 5(c)) and the tri-phase case (Fig. 5(e)). Nevertheless, more meticulous assessment exposes that slight departure is discernible for the bi-phase case which is particularly plotted in the narrower range as shown in Figure 5(d), in contrast to the corresponding almost precise fitting in the tri-phase case as shown in Figure 5(f). Table I summarizes up the relevant fitting parameters, where R^2 is the correlation coefficient and $\beta = k_B T/\mu$, in addition to the conventions as defined above.

We give a brief description of the fitting results. For the single-phase fit, the saturation magnetization M_s, the coercivity H_c and the switching parameter β are, separately, 42.9 emu/g, − 12.3 Oe and 286.4 Oe for the down-field sweeping, and 43.0 emu/g, 13.4 Oe and 293.3 Oe for

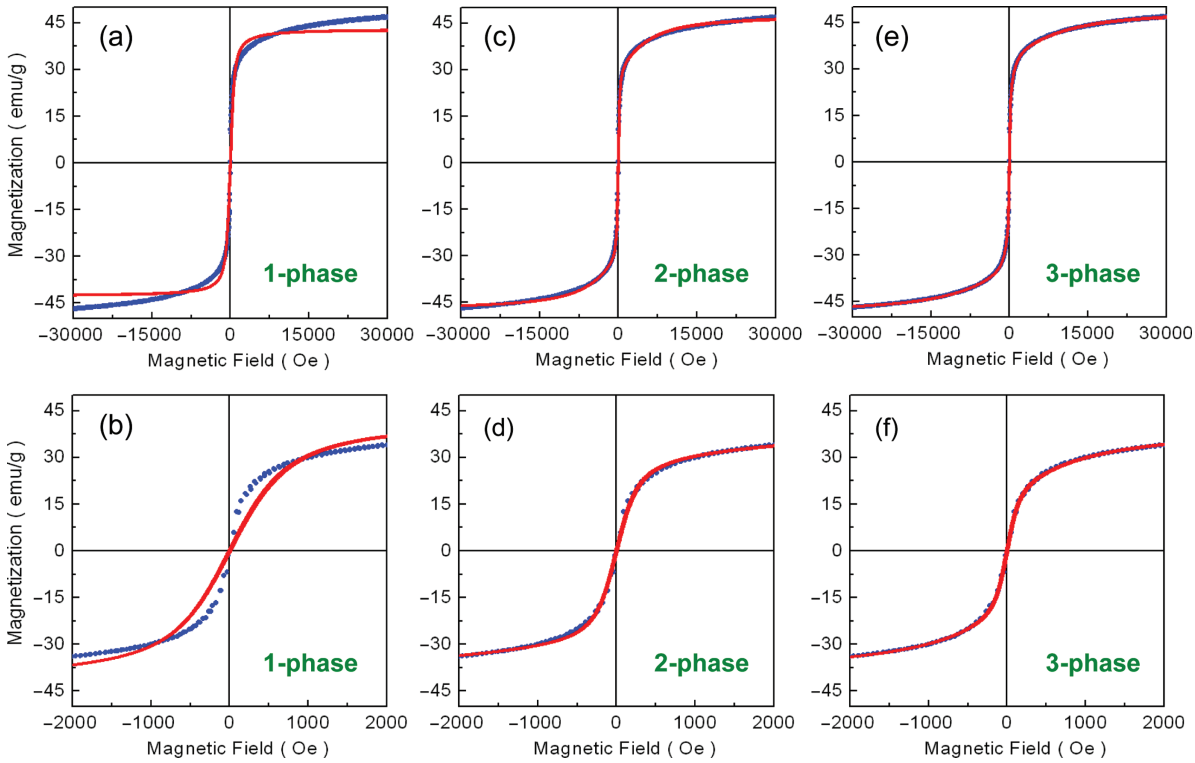

Fig. 5. Magnetic analysis on the hysteresis curves by the modified Langevin equations in two ranges of magnetic field. (a), (b) Single-phase fit, (c), (d) bi-phase fit, and (e), (f) tri-phase fit. Experimental data in dots and fit results in curves.

Table I. Analysis of the hysteresis curves by the modified Langevin equation, with the parameters derived from single-, bi- and tri-phase fittings.

(a) Parameters from the single-phase fit.

	Down-field sweep	Up-field sweep
M_S (emu/g)	42.9 (0.1)	43.0 (0.1)
H_c (Oe)	−12.3 (9.7)	13.4 (9.8)
β (Oe)	286.4 (6.3)	293.3 (6.3)
R^2	0.99445	0.99434
Offset (emu/g)	0.0 (0.1)	0.0 (0.1)

(b) Parameters from the bi-phase fit.

	Down-field sweep		Up-field sweep	
	Phase 1	Phase 2	Phase 1	Phase 2
M_S (emu/g)	32.1 (0.1)	15.9 (0.1)	32.1 (0.1)	15.8 (0.1)
H_c (Oe)	−11.3 (1.3)	−0.7 (27.6)	11.6 (1.4)	−4.7 (27.7)
β (Oe)	105.3 (1.1)	3080.8 (47.0)	107.0 (1.2)	3120.2 (48.0)
R^2	0.99985		0.99985	
Offset (emu/g)	0.0 (0.0)		0.0 (0.0)	

(c) Parameters from the tri-phase fit.

	Down-field sweep			Up-field sweep		
	Phase 1	Phase 2	Phase 3	Phase 1	Phase 2	Phase 3
M_S (emu/g)	23.1 (0.2)	13.4 (0.1)	12.8 (0.0)	23.1 (0.2)	13.3 (0.1)	12.8 (0.0)
H_c (Oe)	−11.2 (0.5)	−17.3 (2.9)	37.7 (22.7)	11.3 (0.5)	13.7 (3.0)	−57.6 (23.8)
β (Oe)	60.9 (0.6)	468.9 (7.2)	5544.9 (55.2)	61.7 (0.7)	476.6 (7.6)	5604.7 (58.0)
R^2		0.99999			0.99999	
Offset (emu/g)		0.0 (0.0)			− 0.1 (0.0)	

Note: Fitting errors in the brackets.

the up-field sweeping. Though the numbers show almost no much difference in both modes of down-field and up-field sweeping, the fitting is far from being adequate, in terms of Figure 5(a) and the correlation coefficients of 0.99445 and 0.99434. For the bi-phase fit, the polymer-coated hybrid-phase iron oxide nanoparticles are separated into one major and one minor magnetic phase. For the down-field sweeping, the values of M_s, H_c and β read 32.1 emu/g, −11.3 Oe and 105.3 Oe for the major magnetic phase and 15.9 emu/g, −0.7 Oe and 3080.8 Oe for the minor magnetic phase, respectively, whereas upon the up-field sweeping they become 32.1 emu/g, 11.6 Oe and 107.0 Oe for the former and 15.8 emu/g, −4.7 Oe and 3120.2 Oe for the latter, correspondingly. Since the bi-phase fit has generated a rather sensible outcome with respective to the slight discrepancy as previously addressed and the correlation coefficients are improved to 0.99985, nonetheless, the standard deviations of the coercivities (27.6 Oe and 27.7 Oe) as given in the table for the minor phase are magnificently large, connoting that more plausible justification is of necessity. In fact, the tri-phase fit as shown in Figures 5(e), (f) has resulted in almost perfect evaluation. In light of the table, the polymer-coated hybrid-phase iron oxide nanoparticles are divided into one major and two minor magnetic phases. For the major phase, the values of M_s, H_c and β are 23.1 emu/g, −11.2 Oe and 60.9 Oe under down-field sweeping, and 23.1 emu/g, 11.3 Oe and 61.7 Oe under up-field sweeping. Correspondingly, the data of the two minor magnetic phases are separately 13.4 emu/g and 12.8 emu/g for M_s, −17.3 Oe and 37.7 Oe for H_c, and 468.9 Oe and 5544.9 Oe for β in the case of down-field sweep, in comparison to the case of up-field sweep which offers 13.3 emu/g and 12.8 emu/g for M_s, 13.7 Oe and −57.6 Oe for H_c, and 476.6 Oe and 5604.7 Oe for β. In addition to the rational standard deviations, the increased correlation coefficients of 0.99999 concurrently proves that, within the error of the measurements, the analysis sustains that the PEO-PPO-PEO-coated nanoparticle system is likely composed of three magnetic phases, in consistence with the XRD and TEM characterization in the precedent sections.[30]

4. CONCLUSION

In summary, we have prepared the hybrid-phase iron oxide nanoparticles laced by the PEO-PPO-PEO triblock copolymer through the one-pot nanoemulsion synthesis. The nanomaterial as prepared comprises three distinct phases, FeO, α-Fe and Fe_3O_4, with the lattice parameters of the new orthorhombic FeO phase given by $a = 8.034$ Å, $b = 10.359$ Å, and $c = 12.341$ Å. In terms of the magnetic measurements, the hybrid-phase iron oxide nanoparticles possess well-defined soft ferromagnetic behaviour, and the corresponding magnetic hysteresis curves are successfully deconvoluted by the modified tri-phase Langevin equation, separating the nanoparticle system into three magnetic phases in match to the structural phases. It is useful to emphasize that the unusual magnetic responses as found in the hybrid nanomaterial are owing to the coexistence of ferromagnetic, ferrimagnetic and antiferromagnetic constituents in the same nanoparticles. As the composition of the material is tuneable by experimental conditions and thus well-behaved magnetic properties, such hybrid-phase iron oxide nanoparticles could be of interest in the research of complex materials and for potential applications in biomedical fields as proved in the cases of Fe_3O_4 nanoparticles studied by us for cell separation and dendritic cell-based cancer immunotherapy.[7, 10]

Acknowledgments: This work was supported in part by the Scientific and Technological Development Projects, Science and Technology Department of Henan Province, China (No. 112300410011), the National Natural Science Foundation of China (No. 51172064), the National Research Foundation of Korea (Nos. 2012-0005657, 2012-0001067), the Industrial Core Technology Development Program funded by the Ministry of Trade, Industry and Energy (No. 10033183), and the Seoul R&BD Program (No. 10920).

References and Notes

1. R. M. Cornell and U. Schwertman, The Iron Oxides: Structure, Properties, Reactions, Occurrences and Uses, Wiley-VCH, Weinheim **(2003)**.
2. H. Ozawa, F. Takahashi, K. Hirose, Y. Ohishi, and N. Hirao, *Science* 334, 792 **(2011)**.
3. S.-B. R. Chang and J. L. Kirschvink, *Ann. Rev. Earth Planet. Sci.* 17, 169 **(1989)**.
4. J. Liu, S. Z. Qiao, Q. H. Hu, and G. Q. Lu, *Small* 7, 425 **(2011)**.
5. L. R. Merte, G. Peng, R. Bechstein, F. Rieboldt, C. A. Farberow, L. C. Grabow, W. Kudernatsch, S. Wendt, E. Lægsgaard, M. Mavrikakis, and F. Besenbacher, *Science* 6083, 889 **(2012)**.
6. P. Xu, G. M. Zeng, D. L. Huang, C. L. Feng, S. Hu, M. H. Zhao, C. Lai, Z. Wei, C. Huang, G. X. Xie, and Z. F. Liu, *Sci. Total Environment* 424, 1 **(2012)**.
7. N. H. Cho, T. C. Cheong, J. H. Min, J. H. Wu, S. J. Lee, D. Kim, J. S. Yang, S. Kim, Y. K. Kim, and S. Y. Seong, *Nat. Nanotechnol.* 6, 675 **(2011)**.
8. Z. Ullah, S. Atiq, and S. Naseem, *J. Alloys Compounds* 555, 263 **(2013)**.
9. A. G. Gupta and M. Gupta, *Biomaterials* 26, 3995 **(2005)**.
10. H. L. Liu, C. H. Sonn, J. H. Wu, K. M. Lee, and Y. K. Kim, *Biomaterials* 9, 4003 **(2008)**.
11. M. Gheisari, M. Mozaffari, M. Acet, and J. Amighian, *J. Magn. Magn. Mater.* 320, 2618 **(2008)**.
12. A. Glaria, M. L. Kahn, P. Lecante, B. Barbara, and B. Chaudret, *ChemPhysChem.* 9, 776 **(2008)**.
13. T. Hyeon, S. S. Lee, J. Park, Y. Chung, and H. H. Na, *J. Am. Chem. Soc.* 123, 12798 **(2001)**.
14. M. Gheisari, M. Mozafari, M. Niyaifar, J. Amighian, and R. Soleimani, *J. Supercond. Nov. Magn.* 26, 237 **(2013)**.
15. G. C. Papaefthymiou, F. X. Redl, C. T. Black, R. L. Sandstrom, M. Yin, C. B. Murray, and S. P. O'Brien, *Hyperfine Interact.* 165, 239 **(2005)**.
16. L. M. Bronstein, X. Huang, J. Retrum, A. Schmucker, M. Pink, B. D. Stein, and B. Dragnea, *Chem. Mater.* 19, 3624 **(2007)**.

17. C. J. Chen, R. K. Chiang, H. Y. Lai, and C. R. Lin, *J. Phys. Chem. C* 114, 4258 **(2010)**.
18. E. Wetterskog, C.-W. Tai, J. Grins, L. Bergstrom, and G. Salazar-Alvarez, *ACS Nano* 7, 7132 **(2013)**.
19. H. L. Liu, P. Hou, W. X. Zhang, and J. H. Wu, *Colloids Surf. A: Physicochem. Eng. Aspects* 356, 21 **(2010)**.
20. H. L. Liu, J. H. Wu, J. H. Min, P. Hou, A. Y. Song, and Y. K. Kim, *Nanotechnology* 22, 055701 **(2011)**.
21. T. K. Jain, S. P. Foy, B. Erokwu, S. Dimitrijevic, C. A. Flask, and V. Labhasetwar, *Biomaterials* 30, 6748 **(2009)**.
22. F. Alexis, E. Pridgen, L. K. Molnar, and O. C. Farokhzad, *Mol. Pharmaceutics.* 5, 505 **(2008)**.
23. J. Yang, Y. Zhai, Y. Deng, D. Gu, Q. Li, Q. Wu, Y. Huang, B. Tu, and D. Zhao, *J. Colloid Interface Sci.* 342, 579 **(2010)**.
24. K. Herve, L. Douziech-Eyrolles, E. Munnier, S. Cohen-Jonathan, M. Souce, H. Marchais, P. Limelette, F. Warmont, M. L. Saboungi, P. Dubois, and I. Chourpa, *Nanotechnology* 19, 465608 **(2008)**.
25. S. Chen, Y. Li, C. Guo, J. Wang, J. Ma, X. Liang, L.-R. Yang, and H.-Z. Liu, *Langmuir* 23, 12669 **(2007)**.
26. K. Nakamoto, Infrared and Raman Spectra of Inorganic and Coordination Complexes, Wiley-VCH, New York **(1978)**.
27. C. Cavelius, K. Moh, and S. Mathur, *Cryst. Growth Des.* 12, 5948 **(2012)**.
28. Y. Ding, H. Liu, J. Xu, C. T. Prewitt, R. J. Hemley, and H.-K. Mao, *Appl. Phys. Lett.* 87, 041912 **(2005)**.
29. B. D. Cullity and S. R. Stock, Elements of X-Ray Diffraction, Prentice Hall, New Jersey **(2001)**.
30. J. H. Wu, *Nanotechnology* 13, 720 **(2002)**.